Complex-valued wavelet lifting and applications

B Supplementary Material: Real nonparametric regression using complex lifting

In this document we examine how to employ complex lifting to denoise irregularly sampled real-valued signals. Let us assume that we are in the nonparametric regression context, where $f_1, \ldots, f_n$ are noisy observations of an unknown function g, taken at possibly *irregularly* spaced locations $x_1, \ldots, x_n$. A popular approach is to model the observations as

$$f_i = g(x_i) + \varepsilon_i, \tag{B.1}$$

where $\varepsilon_1, \ldots, \varepsilon_n$ are random variables that denote the noise, usually assumed to be independently distributed, with zero mean and finite variance, σ^2. The locations $\underline{x} = (x_1, \ldots, x_n)$ are assumed fixed and are usually assumed to span the interval [0,1], so $g : [0, 1] \longrightarrow \mathbb{R}$. The regression problem consists of estimating g. Note that as usual in nonparametric regression problems, we do not assume any functional form for g to assist us in its estimation.

Wavelet approaches to nonparametric regression (Donoho and Johnstone, 1994, 1995) have been shown to perform well in a range of denoising settings. Put simply, the wavelet shrinkage approach consists of decomposing $\underline{f} = (f_1, \ldots, f_n)$ by a DWT into wavelet coefficients, thresholding (somehow) the coefficients with the aim of removing the noise, and then inverting the transform. The function obtained after inversion gives an estimate, $\hat{g}$, for g. In what follows we shall modify this wavelet shrinkage paradigm in order to take advantage of our complex-valued lifting transform. For an approach using classical complex-valued wavelets for denoising real-valued signals, the reader is directed to Barber and Nason (2004).

Our proposed denoising procedure is:

1. Decompose the noisy signal $\underline{f}$ by the proposed $\mathbb{C}$-LOCAAT. In what follows, let us denote the resulting detail (wavelet) vector by $\underline{d}$, obtained as described by equations (1)–(3) in the main article. As the complex-valued lifting transform can be thought of as two lifting schemes, each of which is a linear transform, we can write our transform as $\underline{d} = W^{(c)}\underline{f}$, where the complex lifting matrix $W^{(c)} \in \mathcal{M}_{n\times n}(\mathbb{C})$ can be decomposed into the (real-valued) matrices associated to the two lifting schemes as $W^{(c)} = W^{Re} + \mathrm{i}\, W^{Im}$.

   After application of $\mathbb{C}$-LOCAAT, we obtain $W^{(c)}\underline{f} = W^{(c)}\underline{g} + W^{(c)}\underline{\varepsilon}$, or equivalently using the nonparametric regression formulation (B.1),

$$\underline{d} = \underline{d}^{\star} + \underline{e}^{(c)}. \tag{B.2}$$

   In the above $\underline{d}^{\star} = W^{(c)}\underline{g}$ are the true (unknown) details and $\underline{e}^{(c)} = W^{(c)}\underline{\varepsilon}$ represents the underlying transformed noise. In this setting $\underline{e}^{(c)}$ is a vector of complex-valued random variables and due to the lifting construction, the noise (and consequently the detail coefficients) are now no longer independently distributed but rather have a covariance structure given by $\mathrm{var}(\underline{d}) = \sigma^2 W^{(c)}\overline{W^{(c)}}^{T}$. The correlation between wavelet coefficients is in effect induced by the lifting transform, and is analogous to that found in the real-valued LOCAAT scheme (Nunes et al., 2006). Correlation is also present between the real and imaginary parts of the complex wavelet vector, which we now describe.

Proposition 1. *Let $\underline{e}^{(c)} = W^{(c)}\underline{\varepsilon}$, where $\underline{\varepsilon} \sim N_n(0, \sigma^2 I_n)$ and $W^{(c)} \in \mathcal{M}_{n\times n}(\mathbb{C})$ is a $n \times n$ complex matrix that represents the complex-valued lifting transform. Then the real and imaginary parts of $\underline{e}^{(c)}$*

are normal real-valued random variables with the following covariance structure:

$$\begin{aligned}
\mathrm{var}(Re(\underline{e}^{(c)})) &= \frac{\sigma^2}{2} Re\left(W^{(c)}\overline{W^{(c)}}^T + W^{(c)}(W^{(c)})^T\right) \\
\mathrm{var}(Im(\underline{e}^{(c)})) &= \frac{\sigma^2}{2} Re\left(W^{(c)}\overline{W^{(c)}}^T - W^{(c)}(W^{(c)})^T\right) \\
\mathrm{cov}(Im(\underline{e}^{(c)}), Re(\underline{e}^{(c)})) &= \frac{\sigma^2}{2} Im\left(W^{(c)}\overline{W^{(c)}}^T + W^{(c)}(W^{(c)})^T\right) \\
\mathrm{cov}(Re(\underline{e}^{(c)}), Im(\underline{e}^{(c)})) &= -\frac{\sigma^2}{2} Im\left(W^{(c)}\overline{W^{(c)}}^T - W^{(c)}(W^{(c)})^T\right). \qquad \text{(B.3)}
\end{aligned}$$

Proof. The covariance between the real and imaginary parts of the complex detail coefficient vector, $\mathrm{cov}\left(Im(\underline{e}^{(c)}), Re(\underline{e}^{(c)})\right)$, can be expressed as

$$\begin{aligned}
\mathrm{cov}\left(Im(\underline{e}^{(c)}), Re(\underline{e}^{(c)})\right) &= \mathrm{cov}\left(\frac{\underline{e}^{(c)} - \overline{\underline{e}^{(c)}}}{2\mathrm{i}}, \frac{\underline{e}^{(c)} + \overline{\underline{e}^{(c)}}}{2\mathrm{i}}\right) \\
&= \frac{1}{4\mathrm{i}} \mathrm{cov}\left(\underline{e}^{(c)} - \overline{\underline{e}^{(c)}}, \underline{e}^{(c)} + \overline{\underline{e}^{(c)}}\right) \\
&= \frac{1}{4\mathrm{i}} \left(\mathrm{cov}\left(\underline{e}^{(c)}, \underline{e}^{(c)}\right) + \mathrm{cov}\left(\underline{e}^{(c)}, \overline{\underline{e}^{(c)}}\right) - \mathrm{cov}\left(\overline{\underline{e}^{(c)}}, \underline{e}^{(c)}\right) - \mathrm{cov}\left(\overline{\underline{e}^{(c)}}, \overline{\underline{e}^{(c)}}\right)\right) \\
&= \frac{1}{4\mathrm{i}} \left(\sigma^2 W^{(c)}\overline{W^{(c)}}^T + \sigma^2 W^{(c)} {W^{(c)}}^T - \sigma^2 \overline{W^{(c)}W^{(c)}}^T - \sigma^2 \overline{W^{(c)}} {W^{(c)}}^T\right),
\end{aligned}$$

since $\underline{e}^{(c)} = W^{(c)}\underline{\varepsilon}$, and $\underline{\varepsilon} \sim N_n(0, \sigma^2 I_n)$ is a real-valued vector. Denoting $z_1 = W^{(c)}\overline{W^{(c)}}^T$ and $z_2 = W^{(c)}{W^{(c)}}^T$, the covariance can be written as

$$\begin{aligned}
\mathrm{cov}\left(Im(\underline{e}^{(c)}), Re(\underline{e}^{(c)})\right) &= \frac{\sigma^2}{4\mathrm{i}} \left((z_1 - \overline{z_1}) + (z_2 - \overline{z_2})\right) \\
&= \frac{\sigma^2}{2} \left(Im(z_1) + Im(z_2)\right).
\end{aligned}$$

Substituting the expressions for z_1 and z_2 back into this equation, the covariance is equal to

$$\frac{\sigma^2}{2}\left(Im\left(W^{(c)}\overline{W^{(c)}}^T\right) + Im\left(W^{(c)}{W^{(c)}}^T\right)\right).$$

The expressions for $\mathrm{var}(Re(\underline{e}^{(c)}))$, $\mathrm{var}(Im(\underline{e}^{(c)}))$ and $\mathrm{cov}(Re(\underline{e}^{(c)}), Im(\underline{e}^{(c)}))$ can be established following similar arguments.

□

This result can be seen as generalising Proposition 1 of Barber and Nason (2004).

2. In order to remove the noise, we use a thresholding approach in the multiwavelet spirit, as proposed by Downie and Silverman (1998), see also Barber and Nason (2004). Following the application of $\mathbb{C}$-LOCAAT, the detail coefficient d_{j_k} associated to each observed point may be viewed as a vector $(\lambda_{j_k}, \mu_{j_k})$ following a bivariate normal distribution $d_{j_k} \sim N_2(d^\star_{j_k}, \Sigma_{j_k})$, where Σ_{j_k} is a 2×2 matrix that contains the covariance structure in the wavelet domain associated to the j_kth point. The entries of Σ_{j_k} can be calculated using the equations (B.3) in Proposition 1.

   The thresholding approach suggested in Downie and Silverman (1998) amounts to computing a thresholding statistic $\theta_{j_k} = d^T_{j_k}(\Sigma_{j_k})^{-1} d_{j_k}$, where again we stress that d_{j_k} is understood as a two-dimensional random vector (rather than a complex variable). Under our model assumptions, $\theta_{j_k} \sim \chi^2_2({d^\star_{j_k}}^T(\Sigma_{j_k})^{-1} d^\star_{j_k})$ and this statistic can then be fed into a thresholding procedure. Various thresholding procedures exist for such bivariate vectors in the regular sampling setting, namely hard and soft thresholding rules as

well as bivariate empirical Bayes' thresholding methods, see Barber and Nason (2004) and Fryzlewicz (2007) for more details.

In our denoising procedure in Section B.1 below, we employ a soft thresholding rule as detailed in Downie and Silverman (1998). Each wavelet coefficient d_{j_k} is shrunk-or-killed to obtain $\hat{d}^{\star}_{j_k}$ as $\hat{d}^{\star}_{j_k} = d_{j_k} \cdot \max(\theta_{j_k} - \lambda_j, 0)\,|\theta_{j_k}|^{-1}$. Note that we use a level-dependent threshold $\lambda_j = 2\sigma^2 \log(n_j)$ as opposed to the universal threshold $\lambda = 2\sigma^2 \log(n)$ as proposed by Downie and Silverman (1998). To compute this threshold, we use an artificial level construction to mimic scales produced by a traditional DWT (see Nunes et al. (2006) for more details). The threshold λ_j is then computed using the number of coefficients n_j in the artificial level to which d_{j_k} belongs.

In practice the variance of the original noise (σ^2) also needs to be estimated. We propose two alternative estimators for this. Firstly, in a similar spirit to Nunes et al. (2006), we estimate the noise by $\hat{\sigma}_c = \frac{1}{2}\left(\mathrm{MAD}\left(Re\left(\underline{\tilde{d}}^1\right)\right) + \mathrm{MAD}\left(Im\left(\underline{\tilde{d}}^1\right)\right)\right)$, where $\underline{\tilde{d}}^1$ represent normalised complex detail coefficients $d_j\{\mathrm{diag}(W^{(c)}\overline{W^{(c)}}^T)_j\}^{-1/2}$ identified as lying in the finest artificial level. Alternatively, we use the estimator detailed in Nunes et al. (2006), which amounts to only using the real part of the transform. More specifically, this estimates the noise level by $\hat{\sigma}_{Re} = \mathrm{MAD}(\underline{\tilde{d}}^{Re,1})$, where $\underline{\tilde{d}}^{Re,1}$ represent normalised *real* detail coefficients $Re(d_j)\{\mathrm{diag}(W^{(Re)}W^{(Re)T})_j\}^{-1/2}$. The variance matrix Σ_{j_k} can then be estimated using $\hat{\sigma}^2$ and equations (B.3).

We have found that other thresholding procedures do not perform as well as soft thresholding in the complex lifting setting: whilst in many cases, hard thresholding outperforms competitor methods, it can produce results with visually undesirable artifacts; empirical Bayes procedures suffer from numerical optimization problems in maximizing the likelihood, reflecting similar findings in Barber and Nason (2004).

3. The complex lifting transform is then inverted and the real part of the estimated signal is considered as our desired $\hat{g}$. Note that this follows Barber and Nason (2004) in performing inversion of the (thresholded) real component of the complex wavelet coefficients (using equation (5) in the main article). However, it is important to point out that the imaginary parts of the wavelet coefficients play a crucial role in extracting additional information from data and thus in thresholding (see discussion above), as bivariate thresholding is known to produce lower risk estimates than the univariate version.

B.1 Simulation study

In this section we assess the performance of our proposed method against that of state-of-the-art competitor methods. The denoising performance of our estimator will be tested on the test functions *Blocks*, *Bumps*, *HeaviSine* and *Doppler* (Donoho and Johnstone, 1994), and on the *Ppoly* function (Nason and Silverman, 1994). These test functions model various features of signals that arise in practical applications, see e.g. Nason (2008) for more details.

The irregular sampling locations $\underline{x} = \{x_i\}_{i=1}^{n=256}$ are generated by 'jittering' a regular grid on the interval [0,1] (Nunes et al., 2006). For comparability with the results in Nunes et al. (2006) and with techniques that only work on regular observations, we use grids with three (increasing) degrees of irregularity, $d_1 = 0.01, d_2 = 0.1$ and $d_3 = 1$. As customary, the true signal $(\underline{x}, \underline{g})$ is contaminated with additive noise, $\varepsilon \sim N(0, \sigma_\varepsilon^2)$. The signal-to-noise ratio $\mathrm{SNR} = \sqrt{\mathrm{var}(\underline{g})}/\sigma_\varepsilon$ takes values 3, 5 and 7.

In order to quantify the performance of each method, for each grid type and level of noise we performed the denoising procedure $K = 100$ times. A measure of the overall accuracy of the estimates is given by the estimated average mean square error,

$$\mathrm{amse} = (nK)^{-1} \sum_{k=1}^{K} \sum_{i=1}^{n} (\hat{g}_i^{(k)} - g_i^{(k)})^2.$$

We compared our method against the successful real-valued adaptive lifting scheme AP1S of Nunes et al. (2006) (referred to as '$\mathbb{R}$-lift' in the tables below). For completeness, we reproduce the results for *Locfit* local

regression method (Loader, 1997, 1999), spline smoothing with cross-validation (SSCV) and the Kovac-Silverman (KS) wavelet procedure (Kovac and Silverman, 2000) from tables in Nunes et al. (2006).

We report results using a linear regression order in the *predict* step of the $\mathbb{C}$-LOCAAT algorithm, and denote this by $\mathbb{C}$-LP1S. As already mentioned in Section 2.2, we also propose the use of the adaptive filter AP1S of Nunes et al. (2006) as our lead filter $\mathbf{L}$. This amounts to building an *adaptive* complex-valued lifting scheme, referred to as $\mathbb{C}$-AP1S in subsequent text. Table 1 also reports on the performance of the (univariate) complex nondecimated lifting transform using the adaptive filter AP1S (denoted $\mathbb{C}$NLT-AP1S) and $P = 50$ trajectories.

Simulation results. Table 1 shows the denoising performance of our proposed procedure against competitor methods described above. Overall, our method performs very well.

Table B.1: AMSE ($\times 10^3$) simulation results for test signals with SNR=3 with three levels of jitter, d, for various denoising methods described in the text. For the reported $\mathbb{C}$NLT results, $P = 50$ trajectories were used.

	Blocks			*Bumps*			*HeaviSine*			*Doppler*			*Ppoly*		
Method	d_1	d_2	d_3	d_1	d_2	d_3	d_1	d_2	d_3	d_1	d_2	d_3	d_1	d_2	d_3
$\mathbb{R}$-lift	72	68	59	77	77	62	20	20	23	52	50	48	16	17	18
$\mathbb{C}$-LP1S $\hat{\sigma}_c$	36	34	35	53	53	48	21	21	23	44	45	44	17	16	18
$\mathbb{C}$-LP1S $\hat{\sigma}_{Re}$	45	44	42	78	77	65	18	17	18	53	53	51	12	11	13
$\mathbb{C}$-AP1S $\hat{\sigma}_c$	32	33	32	51	50	48	22	22	23	45	44	44	17	16	18
$\mathbb{C}$-AP1S $\hat{\sigma}_{Re}$	37	39	34	70	69	54	18	18	19	49	49	46	12	12	13
Locfit	73	72	64	110	108	101	11	11	11	58	58	54	21	20	19
SSCV	74	74	67	307	315	250	12	11	12	61	60	53	20	20	19
KS	79	78	87	179	181	259	13	12	15	51	52	57	18	17	18
$\mathbb{C}$NLT-AP1S $\hat{\sigma}_c$	27	26	27	45	44	42	18	18	19	42	40	42	13	13	14
$\mathbb{C}$NLT-AP1S $\hat{\sigma}_{Re}$	33	31	28	62	60	46	15	15	17	48	46	43	9	9	11

Table B.2: AMSE ($\times 10^3$) simulation results for test signals with SNR=5 with three levels of jitter, d, for various denoising methods described in the text. For the reported $\mathbb{C}$NLT results, $P = 50$ trajectories were used.

	Blocks			*Bumps*			*HeaviSine*			*Doppler*			*Ppoly*		
Method	d_1	d_2	d_3	d_1	d_2	d_3	d_1	d_2	d_3	d_1	d_2	d_3	d_1	d_2	d_3
AP1S	22	23	20	30	29	23	10	10	10	22	22	21	6	6	7
$\mathbb{C}$-LP1S $\hat{\sigma}_c$	13	13	13	18	18	18	9	9	10	21	21	20	7	7	7
$\mathbb{C}$-LP1S $\hat{\sigma}_{Re}$	16	16	15	25	26	22	8	8	9	24	24	23	5	5	5
$\mathbb{C}$-AP1S $\hat{\sigma}_c$	13	12	12	18	18	17	10	9	10	21	20	19	7	7	7
$\mathbb{C}$-AP1S $\hat{\sigma}_{Re}$	14	14	13	24	22	19	9	8	9	23	22	20	5	5	5
Locfit	35	35	34	40	40	39	7	7	7	25	26	25	12	12	11
SSCV	51	51	46	277	285	227	7	7	7	37	37	30	11	12	11
KS	52	52	59	130	134	213	8	7	8	29	28	33	9	9	10
$\mathbb{C}$NLT-AP1S $\hat{\sigma}_c$	10	9	10	15	15	16	8	8	9	18	18	19	5	5	6
$\mathbb{C}$NLT-AP1S $\hat{\sigma}_{Re}$	10	10	10	19	19	17	7	7	8	20	19	19	4	4	5

Examination of the simulation results shows that the proposed denoising procedure yields excellent performance for the signals *Blocks* and *Bumps*, which are known to be difficult to denoise, with a percentage improvement over (the best) competitors, ranging between 50%–60% for *Blocks* and 23%–35% for *Bumps* in a high noise setting (SNR=3). The reason for this improvement over the real-valued lifting procedure is that bivariate thresholding such as we use here almost always produces a lower risk than that of univariate thresholding (see Fryzlewicz (2007, Section 2) in the standard wavelet context).

Notably, the overcomplete adaptive complex lifting transform ($\mathbb{C}$NLT-AP1S) yields a marked improvement over the already appealing $\mathbb{C}$-AP1S, even when bootstrapped over a small number of trajectories.

Table B.3: AMSE ($\times 10^3$) simulation results for test signals with SNR=7 with three levels of jitter, d, for various denoising methods described in the text. For the reported $\mathbb{C}$NLT results, $P = 50$ trajectories were used.

	Blocks			*Bumps*			*HeaviSine*			*Doppler*			*Ppoly*		
Method	d_1	d_2	d_3	d_1	d_2	d_3	d_1	d_2	d_3	d_1	d_2	d_3	d_1	d_2	d_3
AP1S	10	10	10	15	14	12	6	6	6	12	12	11	3	3	4
$\mathbb{C}$-LP1S $\hat{\sigma}_c$	7	7	7	9	9	9	5	5	6	12	12	11	4	4	4
$\mathbb{C}$-LP1S $\hat{\sigma}_{Re}$	8	8	8	12	11	11	5	5	5	13	13	13	3	3	3
$\mathbb{C}$-AP1S $\hat{\sigma}_c$	7	7	7	9	9	9	5	5	6	12	12	11	4	4	4
$\mathbb{C}$-AP1S $\hat{\sigma}_{Re}$	7	7	7	11	11	10	5	5	5	12	12	11	3	3	3
Locfit	20	20	19	21	20	20	5	5	5	13	13	16	9	9	8
SSCV	44	44	39	269	273	220	5	5	5	30	30	23	8	8	8
KS	45	45	52	119	122	195	6	6	5	22	22	25	5	5	6
$\mathbb{C}$NLT-AP1S $\hat{\sigma}_c$	5	5	5	8	8	8	5	5	5	10	11	11	3	3	3
$\mathbb{C}$NLT-AP1S $\hat{\sigma}_{Re}$	5	5	5	9	9	8	4	4	5	10	11	10	2	2	3

In the high noise setting (SNR=3), the amse improvement over the $\mathbb{C}$-AP1S procedure stands at approximately 16% for *Blocks*, 12% for *Bumps*, 30% for *HeaviSine*, 6% for *Doppler* and 15–25% for *Ppoly*. For the smoother *HeaviSine* and *Ppoly* corrupted with milder levels of noise (SNR=5 or SNR=7), the performance of $\mathbb{C}$NLT-AP1S matches or slightly exceeds that of *Locfit* or SSCV methods, designed to deal with smooth signals.

Figure B.1 shows an example of the denoising performance for the *Bumps* signal for SNR=3. Visually, the estimate of the underlying function appears quite similar across the real and complex-valued lifting. However, our proposed complex-valued methods are able to pick out more of the features of the signals, most importantly around the peaks of the *Bumps* signal.

Table B.4 shows simulations results for the test signals described in the text for different numbers of bootstrap trajectories, P. Our investigations on the effect of the number of bootstrap trajectories in the nonparametric regression context shows that, similar to the real-valued LOCAAT in Knight and Nason (2009), the improvement from increasing the number of bootstrap trajectories plateaus for $P > 30$.

Table B.4: AMSE ($\times 10^3$) simulation results for test signals with SNR=3 with three levels of jitter, d, for various denoising methods described in the text, and different numbers of trajectories, P.

	Blocks			*Bumps*			*HeaviSine*			*Doppler*			*Ppoly*		
Method	d_1	d_2	d_3	d_1	d_2	d_3	d_1	d_2	d_3	d_1	d_2	d_3	d_1	d_2	d_3
$\mathbb{C}$NLT-AP1S $\hat{\sigma}_c$ ($P = 10$)	28	27	29	47	45	44	19	19	20	42	42	42	14	13	14
$\mathbb{C}$NLT-AP1S $\hat{\sigma}_{Re}$ ($P = 10$)	34	33	31	63	62	50	16	16	17	48	48	43	10	9	11
$\mathbb{C}$NLT-AP1S $\hat{\sigma}_c$ ($P = 20$)	27	28	27	44	45	42	19	18	19	42	42	42	14	13	14
$\mathbb{C}$NLT-AP1S $\hat{\sigma}_{Re}$ ($P = 20$)	32	33	29	61	59	46	15	15	17	48	46	43	10	9	10
$\mathbb{C}$NLT-AP1S $\hat{\sigma}_c$ ($P = 30$)	27	26	28	45	44	43	18	19	19	41	41	42	13	13	13
$\mathbb{C}$NLT-AP1S $\hat{\sigma}_{Re}$ ($P = 30$)	32	31	29	62	59	48	15	15	17	47	47	42	9	9	10
$\mathbb{C}$NLT-AP1S $\hat{\sigma}_c$ ($P = 50$)	27	26	27	45	44	42	18	18	19	42	40	42	13	13	14
$\mathbb{C}$NLT-AP1S $\hat{\sigma}_{Re}$ ($P = 50$)	33	31	28	62	60	46	15	15	17	48	46	43	9	9	11
$\mathbb{C}$NLT-AP1S $\hat{\sigma}_c$ ($P = 75$)	26	27	27	43	44	41	18	18	19	41	41	41	13	13	13
$\mathbb{C}$NLT-AP1S $\hat{\sigma}_{Re}$ ($P = 75$)	31	33	28	60	59	45	15	15	16	47	46	42	9	9	10
$\mathbb{C}$NLT-AP1S $\hat{\sigma}_c$ ($P = 100$)	26	27	27	43	44	41	18	18	19	41	41	41	13	13	13
$\mathbb{C}$NLT-AP1S $\hat{\sigma}_{Re}$ ($P = 100$)	31	32	28	60	58	45	15	15	16	47	46	42	9	9	10

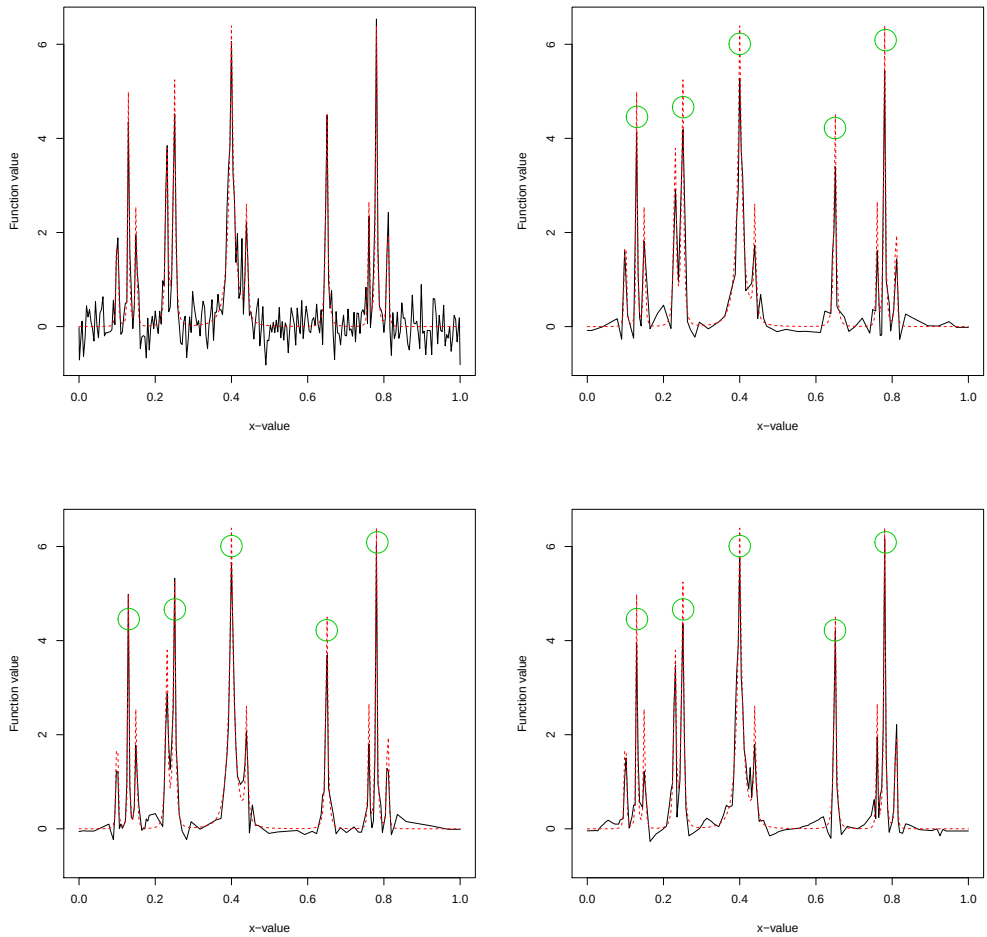

Figure B.1: Examples of denoising a Bumps signal contaminated with noise of SNR = 3. Top-left: the noisy signal; top-right: denoising with $\mathbb{R}$-lift; bottom-left: adaptive complex lifting denoising (our proposed $\mathbb{C}$-AP1S procedure); bottom-right: denoising with our proposed $\mathbb{C}$NLT-AP1S procedure (P=50 trajectories). The dotted function shows the true signal, sampled at $n = 256$ irregular locations.

References

Barber, S. and G. P. Nason (2004). Real nonparametric regression using complex wavelets. *Journal of the Royal Statistical Society B 66*(4), 927–939.

Donoho, D. L. and I. M. Johnstone (1994). Ideal spatial adaptation by wavelet shrinkage. *Biometrika 81*(3), 425–455.

Donoho, D. L. and I. M. Johnstone (1995). Adapting to unknown smoothness via wavelet shrinkage. *Journal of the American Statistical Association 90*, 1200–1224.

Downie, T. R. and B. W. Silverman (1998). The discrete multiple wavelet transform and thresholding methods. *IEEE Transactions on Signal Processing 46*(9), 2558–2561.

Fryzlewicz, P. (2007). Bivariate hard thresholding in wavelet function estimation. *Statistica Sinica 17*(4), 1457–1481.

Knight, M. I. and G. P. Nason (2009). A 'nondecimated' lifting transform. *Statistics and Computing 19*, 1–16.

Kovac, A. and B. W. Silverman (2000). Extending the scope of wavelet regression methods by coefficient-dependent thresholding. *Journal of the American Statistical Association 95*(449), 172–183.

Loader, C. (1997). Locfit: an introduction. *Statistical Compututing and Graphical Newsletters 8*, 11–17.

Loader, C. (1999). *Local Regression and Likelihood*. Springer: New York.

Nason, G. and B. W. Silverman (1994). The discrete wavelet transform in s. *Journal of Computational and Graphical Statistics 3*(2), 163–191.

Nason, G. P. (2008). *Wavelet Methods in Statistics with R*. Springer.

Nunes, M. A., M. I. Knight, and G. P. Nason (2006). Adaptive lifting for nonparametric regression. *Statistics and Computing 16*(2), 143–159.